Available online at www.sciencedirect.com
SCIENCE DIRECT®
Field Crops Research 94 (2005) 126–148
Field Crops Research
www.elsevier.com/locate/fcr

Assessment of durum wheat yield using visible and near-infrared reflectance spectra of canopies

J.P. Ferrio[a], D. Villegas[b], J. Zarco[b], N. Aparicio[b], J.L. Araus[c], C. Royo[b,*]

[a]*Departament de Producció Vegetal i Ciencia Forestal, Universitat de Lleida, Rovira Roure 191, 25198 Lleida, Spain*
[b]*IRTA, Àrea de Conreus Extensius, Centre UdL-IRTA, Rovira Roure 191, 25198 Lleida, Spain*
[c]*Unitat de Fisiología Vegetal, Facultat de Biologia, Universitat de Barcelona, Diagonal 645, 08028 Barcelona, Spain*

Received 29 July 2004; received in revised form 30 November 2004; accepted 20 December 2004

Abstract

The estimation of grain yield before harvesting could be a very useful tool for breeding programs and productivity forecasting. Canopy reflectance indices have been used for yield estimation, but with limited success. This work was carried out to study the suitability of the visible and near-infrared reflectance spectrum of the canopy for the assessment of grain yield in a set of durum wheat genotypes. Five field experiments, each one including 25 genotypes, were conducted in low, medium and high productivity environments, with average yields of 2.5, 4.5 and 7 t/ha. Spectral reflectance measurements between 400 and 1000 nm were made at anthesis and milk-grain stages. Partial least squares regression (PLSR) was used in the construction of models that were tested by simple regression between genotype means of predicted and observed grain yields. The empirical models for the estimation of grain yield showed generally stronger and more robust assessment of grain yield than previously assayed spectral indices. For the best model, correlation coefficients between genotype means of predicted and measured yield within each of the five environments ranged from 0.53 to 0.76. We concluded that, although the models did not provide an accurate quantification of grain yield, they could still be used to rank genotypes for breeding purposes. The most reliable ranking of genotypes was attained using measurements made at milk-grain stage on medium to high productivity environments.

Keywords: Canopy reflectance; PLSR; Anthesis; Milk-grain; Multivariate analysis; Breeding spectroradiometry

1. Introduction

Empirical breeding, based on selection of yield per se, has been very effective in raising wheat productions in the past. Nevertheless, the assessment of grain yield requires the harvest of the experimental plots, which is expensive and time-consuming when it has to be done in the large sets of genotypes that are usually managed by plant breeders. The estimation of plots productivity in a non-destructive way before harvesting would be a very useful tool for selection, mainly in the early generations of a breeding program.

* Corresponding author. Tel.: +34 973 70 25 83; fax: +34 973 23 83 01.
E-mail address: conxita.royo@irta.es (C. Royo).

0378-4290/$ – see front matter © 2004 Elsevier B.V. All rights reserved.
doi:10.1016/j.fcr.2004.12.002

The measurement of the spectral signature of crop canopies at visible and near-infrared (VIS/NIR) regions of the electromagnetic spectrum has shown to be useful to monitor crop growth conditions (Bauer, 1975; Walburg et al., 1982). Spectral reflectance measurements have been successfully used to estimate biomass, leaf area index, photosynthesis and/or yield in several species of trees (Gamon et al., 1995; Richardson et al., 2001), rice (Vaesen et al., 2001), barley (Bort et al., 2002), bread wheat (Filella et al., 1995) and durum wheat (Aparicio et al., 2000, 2002, 2004; Royo et al., 2003).

To manage the information given by the spectrum, vegetation indices, defined as simple operations between reflectance values at given wavelengths, are often used (Field et al., 1994). Some indices are related to the photosynthetic active biomass, such as the normalized difference vegetation index (NDVI), or the simple ratio (SR, see Peñuelas et al., 1997a), both being widely used. Vegetation indices have been used to estimate biomass (Aparicio et al., 2002) and yield (Aparicio et al., 2000) of durum wheat, but phenotypic correlation coefficients found are usually weak and largely dependent on the range of variation of the tested material (Royo et al., 2003). Thus, studies based on comparison among several species have shown much promising results (Peñuelas et al., 1995a, 1997b; Gamon et al., 1997) than those obtained when comparing genotypes of a given species under a single environment (Royo et al., 2003), unless a gradient of variation is introduced in the environment due to, e.g. fertilization (Serrano et al., 2000; Vaesen et al., 2001) or salinity (Peñuelas et al., 1997a). To overcome this problem, some authors have tried to integrate the information given by each index separately by analyzing all them together, obtaining interesting relationships between a combination of indices and chlorophyll concentrations (Filella et al., 1995). Raun et al. (2001) proposed to add NDVI values collected at Feekes growth stages 4 and 5 and divide the result by the GDD between readings to obtain an indication of the potential grain yield of winter wheat, although in a wide range of growing conditions and planting times.

In such context, it becomes useful to study the VIS/NIR spectrum and try to relate all its intrinsic information into a model to estimate genotype variability (i.e. within a species and environment) in important traits such as yield. However, since the potential chemical and physiological basis of the link between grain yield and the whole reflectance spectra of the canopy is not fully understood, empirical calibration is needed to model grain yield from raw spectral data. For empirical calibration using spectral data, multivariate approaches, like partial least squares regression (PLSR), are the most recommended (Beebe and Kowalski, 1987; Martens and Naes, 1991). PLSR decomposes the variability of the spectrum matrix into a number of factors that are not optimal for describing this matrix, but are rotated to simultaneously describe the variable to regress. Therefore, it is especially suitable for this approach, as the main sources of variation in reflectance spectrum are different from those directly associated with grain yield.

The objective of this work was to study the suitability of the VIS/NIR reflectance spectrum of the canopy to assess grain yield of a set of durum wheat genotypes. Additional objectives were to determine the influence of environment, through definition of which environment was more adequate to apply this technique, as well as the predictive value of a model calibrated within a given environment when applied to another one. Finally, we studied the influence of the phenological stage in which the spectra were taken on the ability to assess grain yield.

2. Materials and methods

2.1. Experimental setup

Five field experiments were carried out at three sites of northeastern Spain in 1998 and 1999 (see details in Table 1). Each experiment consisted of 25 durum wheat genotypes sown in a randomized complete block design with four replicates, in plots of 12 m^2 (six rows, 20 cm apart). The genotypes included four commercial Spanish cultivars (Altar-aos, Jabato, Mexa and Vitrón) and 21 advanced lines of the CIMMYT/ICARDA durum wheat breeding program (Awalbit, Bicrecham-1, Chacan, Chahra-1, Haurani, Korifla, Krs/Haucan, Lagost-3, Lahn/Haucan, Massara-1, Moulchahba-1, Mousabil-2, Omlahn-3, Omrabi-3, Omruf-3, Quadalete//Erp/Mal, Sebah, Stojocri-3, Waha, Zeina-1 and Zeina-2).

Table 1
Description and main agronomical characteristics of the sites where trials were performed, including mean yield values achieved

	El Canós		Gimenells		Palau d'Anglesola
Coordinates	41°41′N, 1°13′E		41°40′N, 0°20′E		41°39′N, 1°12′E
Altitude (m above the sea level)	440		200		200
Soil type (USDA)	Fluventic-Xerochrept		Calcixerolic-Xerochrept		Aquic-Xerofluvent
Soil texture	Loamy-fine		Fine-loamy		Fine-loamy
	1998	1999	1998	1999	1999
Sowing date	17 November 1997	3 November 1998	23 November 1997	19 November 1998	10 November 1998
Total rainfall received by the crop (mm)	183	256	285	293	255
Total irrigation (mm)	0	0	100	100	150
Mean temperature (°C)	9.8	10.0	10.3	11.6	9.6
Yield (average ± standard error, kg ha^{-1})	2531 ± 56	3820 ± 111	5202 ± 181	4052 ± 77	7009 ± 73
Productivity classification	Low	Medium	Medium	Medium	High
Trial code	LR (low productivity, rainfed 1998)	MR (medium productivity, rainfed 1999)	MI1 (medium productivity, irrigated 1998)	MI2 (medium productivity, irrigated 1999)	HI (high productivity, irrigated 1999)

The genotypes were chosen to represent a wide range of genetic variability in terms of agronomical characteristics. Seed rate was adjusted to 550 viable seeds m^{-2}. Soil analyses were done prior to sowing, and appropriate fertilization was provided according to the common agronomical practices at each site. Weeds and diseases were controlled, when necessary, using chemicals.

The experiments were classified according to their productivity as: low, medium and high, corresponding to average yields of 2500, 4500 and 7000 kg ha^{-1}, respectively. Low productivity class consisted on one experiment conducted in 1998 under rainfed conditions (LR, see Table 1). Medium productivity class included three experiments, one of which was conducted in 1999 under rainfed conditions and two with supplementary irrigation in 1998 and 1999 (MR, MI1, MI2, respectively). High productivity class consisted of one experiment conducted in 1999 under irrigation (HI). All irrigated experiments were flooded-irrigated and 50 mm were applied 2–3 times at monthly intervals (see Fig. 1). The inclusion of MR environment on medium productivity class was made because of the relatively high yields obtained in this experiment, mainly due to the rains fell in March, April and May, when most of the yield components are determined in these environments.

2.2. Data recorded

Canopy reflectance was measured with a narrow-bandwidth visible-near-infrared portable field spectroradiometer fitted with an 18° field-of-view optic (FieldSpec UV/VNIR, Analytical Spectral Devices, Boulder, CO, USA) as described in Aparicio et al. (2000). The instrument detects 512 continuous bands (with a sampling interval of 1.4 nm) from 350 to 1050 nm wavelengths, thereby covering the visible and near-infrared portion of the spectrum. Measurements were taken with the sensor placed on a vertical rod to take reading from a nadir position, with the sensor raised 2 m above the ground. The measurements were made at midday under cloudless conditions. Three readings (1–2 s each), each being the average of five scans, were made on three different portions of each plot. The reflectance spectrum was calculated in real time as the ratio between the reflected and incident spectra of the canopy. The incident spectrum was obtained every five plots (every minute approximately), from the light reflected by a white reference panel with a very close to Lambertian surface (Spectralon, Labsphere, North Sutton, NH).

Spectral reflectance measurements were made at mid-anthesis and milk-grain stages, corresponding to stages 65 and 75 of the Zadoks' scale (Zadoks et al.,

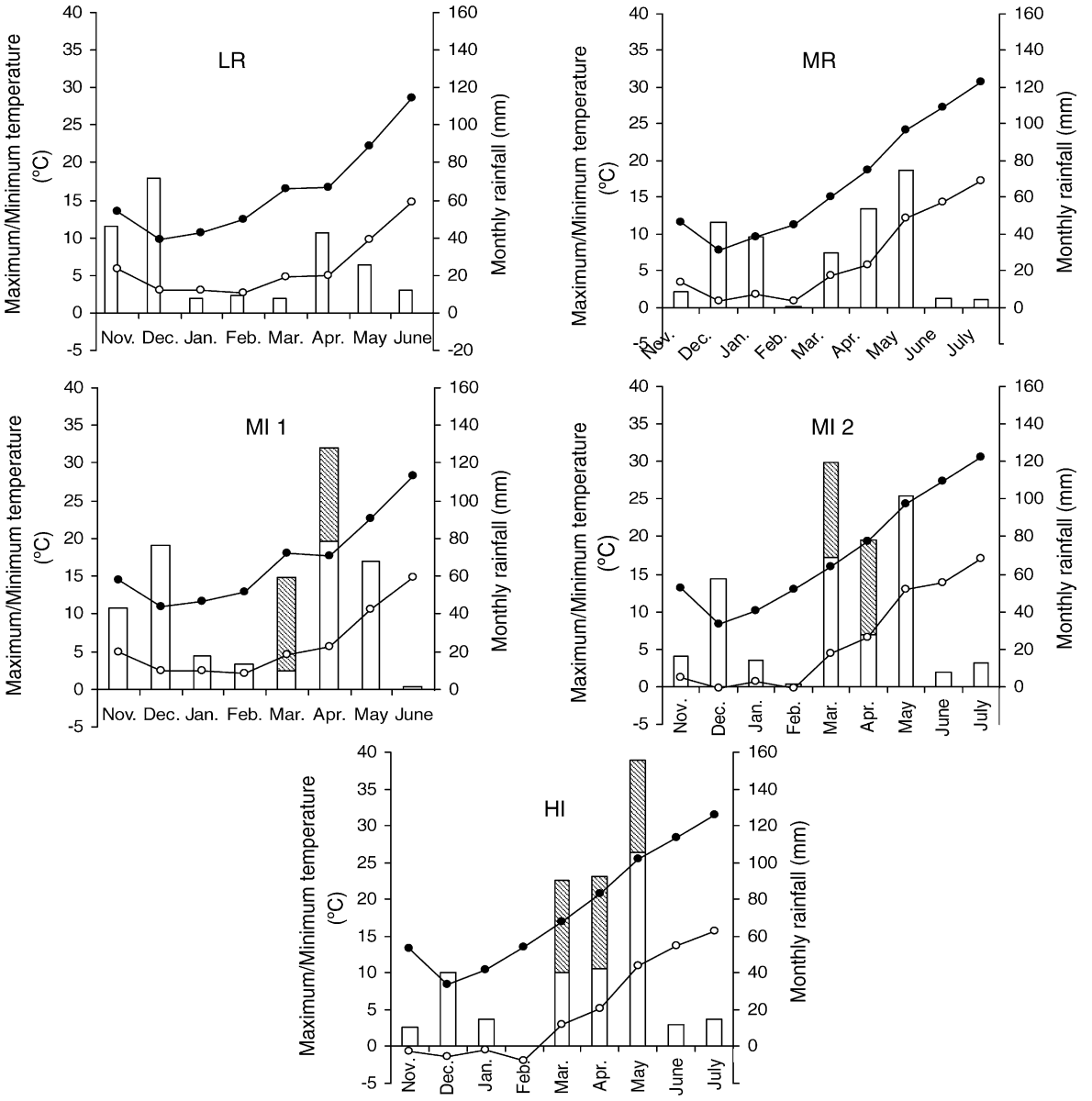

Fig. 1. Monthly minimum (○) and maximum (●) temperatures, rainfall (white bars) and irrigation (striped bars) for each trial: LR, low productivity under rainfed conditions (year 1998) MR, medium productivity under rainfed conditions (1999); MI1, medium productivity under irrigation (1998); MI2, medium productivity under irrigation (1999); and HI, high productivity under irrigation (1999). See more details about the trials in Table 1.

1974), respectively. Plots were harvested mechanically at ripening, and grain yield (kg ha^{-1}) was determined on a plot basis of 12 m^2 and is reported at a 10% moisture level.

2.3. Model construction and validation

Spectra were imported into the program Unscrambler, version 6.0 (CAMO Ltd., New Market,

United Kingdom) that included the PLSR algorithms used in the construction of models. Only spectral bands between 400 and 1000 nm were included in the models, as the spectra outside these limits were noisier and less sensitive. To correct baseline shifts, which are often associated with structural effects, spectra were mean-centered, but not scaled, using the standard normal variate (SNV) algorithm (Barnes et al., 1989). We used all the samples (plots) within each of the trials to calibrate the models. The models were named according to the calibration environment (LR, MR, MI1, MI2, HI), but adding a number to indicate the phenological stage of measurement (6 for anthesis, 7 for milk-grain). We also assayed models calibrated with genotype means within each trial, but they showed poorer performance. The number of PLSR factors used in each model was determined by full cross-validation (Wold, 1978). It consists in building as many models as plots comprised on each trial, each one calibrated leaving out data of one plot from the same trial to be validated. The optimum number of factors was determined by minimizing the root mean standard error (RMSE):

$$\mathrm{RMSE} = \sqrt{\frac{\sum (Y_{\mathrm{ref}} - Y_{\mathrm{est}})^2}{N-1}}$$

where N is the number of samples, Y_{ref} are the observed values of grain yield, and Y_{est} the values estimated from spectral models. However, RMSE did not allow comparing the predictive ability within trials with different grain yield variability. Thus, we also calculated the relative RMSE (rRMSE), defined as the ratio between RMSE and the standard error of grain yield within each trial. The lower the ratio, the greater the ability of the model to detect differences in grain yield within the trial. The resulting regression coefficients for all the models used in this study are plotted in Appendix A.

The robustness of the models was further tested by applying them to the spectra acquired in different experiments. As this work was focused on the prediction of grain yield in breeding programs, we assessed the relationship between genotype means of predicted and measured values by simple regression. We took cross-validation values to estimate the validation performance of the model within the trial used for calibration. Finally, we calculated broad-sense heritabilities (H^2) of measured grain yield and the values estimated by the models, using variance components obtained from the MIXED procedure of SAS statistical package (SAS Institute Inc., 1987). This would indicate to what extent the models were able to track genotypic variability in grain yield.

3. Results

3.1. Spectral features related with grain yield and main wavelengths included in the models

Plots with higher grain yield (GY) showed lower SNV reflectance in the green-red region (500–700 nm) than low-yielding plots, as exemplified in Fig. 2. In contrast, the reflectance in the near-infrared (>700 nm) was higher, with the notable exception of the bands between 950 and 1000 nm. The slope for the increase of reflectance from red to near-infrared (red edge, λ_{RE}) was higher in high-yielding than in low-yielding plots, and shifted towards the near-

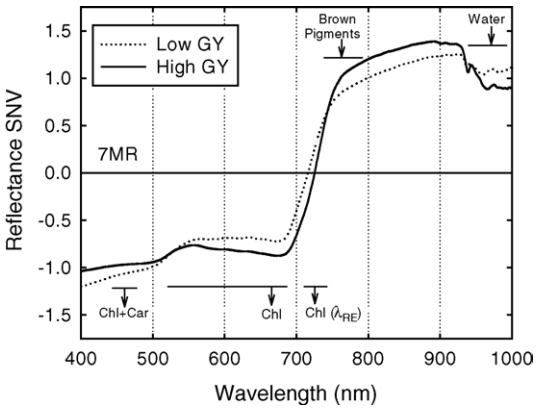

Fig. 2. Mean SNV spectra of the 10 plots of lower and higher GY from the medium-yielding rainfed trial at the milk-grain stage (7MR). Main spectral regions are outlined (see text for further details). Chl + Car, absorption bands shared by chlorophylls and carotenoids; Chl, spectral region with chlorophyll absorption not shared by carotenoids; Chl (λ_{RE}), wavelength of maximum slope in the increase of reflectance from red to near-infrared (red edge); brown pigments, wavelength region absorbed by brown pigments; water, near-infrared region affected by tissue water content. Arrows indicate the sense for increasing content of the referred compounds.

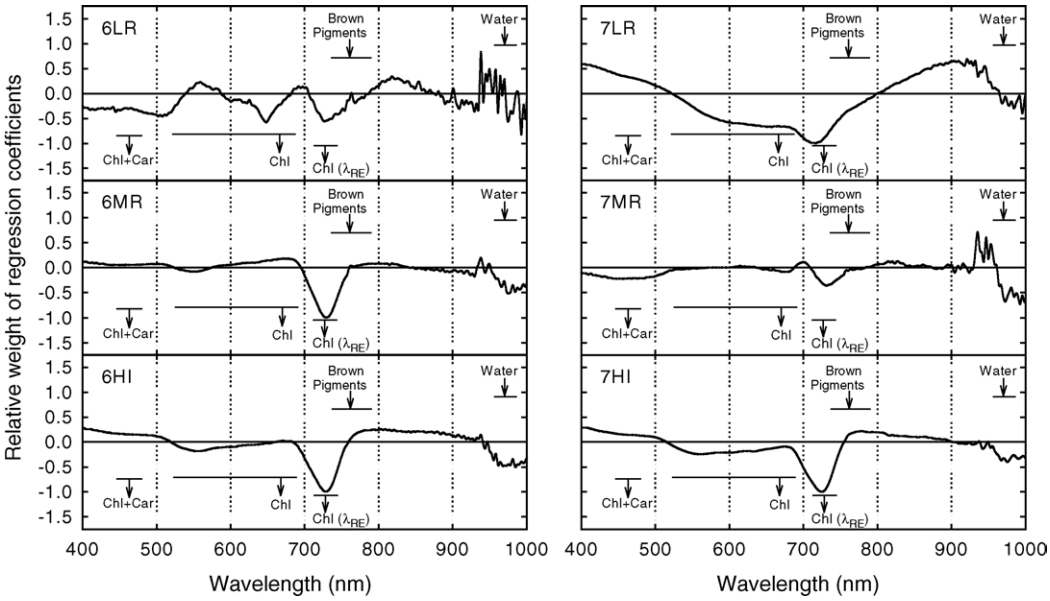

Fig. 3. Regression coefficients for each wavelength, resulting from the models calibrated in three different trials at two developmental stages. In order to make comparisons easier, coefficients have been re-scaled, dividing them by the maximum absolute value for each model. Main spectral regions are outlined (see text for further details). 6LR, 6MR, 6HI, stand for models developed from anthesis data in low-yielding, medium-yielding (rainfed) and high-yielding trials; 7LR, 7MR, 7HI, models developed from milk-grain data in the same trials; Chl + Car, absorption bands shared by chlorophylls and carotenoids; Chl, spectral region with chlorophyll absorption not shared by carotenoids; Chl (λ_{RE}), wavelength of maximum slope in the increase of reflectance from red to near-infrared (red edge); brown pigments, wavelength region absorbed by brown pigments; water, near-infrared region affected by tissue water content. Arrows indicate the sense for increasing content of the referred compounds.

infrared region. Finally, we found that reflectance in high-yielding plots was generally higher in the blue range, between 400 and 500 nm.

Regression coefficients (i.e. the matrix product of the weight given to each PLSR factor and its corresponding wavelength loadings) obtained from PLSR calibration (Fig. 3) were coherent with these spectral patterns. Although there were differences among environments and/or growth stages in the relative contribution to the models of each wavelength, we found several common features. All the models showed high negative coefficients in the left side of the red edge region (700–750 nm). We also found consistent negative coefficients for the wavelengths between 950 and 1000 nm. Some models also included positive coefficients around 800–900 nm (6LR, 6HI, 7LR, 7HI), whereas between 400 and 500 nm we found either positive (6HI, 7LR, 7HI) or negative (6LR, 7MR) coefficients.

3.2. Models construction and calibration performance

Data of each individual plot were used for model construction. The results showed that PLSR reflectance models explained between 20 and 81% of within trial grain yield variability (Table 2). Although estimated yield was always significantly correlated with observed grain yield, this relationship was stronger for low- and medium-yield environments. Calibration RMSE ranged from 253 to 997 kg ha^{-1}, whereas rRMSE varied between 4.4 and 8.9. Generally, RMSE and rRMSE were greater in medium and high-yield trials. Cross-validation performance was somewhat poorer than calibration results, but still showed a significant relationship between predicted and measured values (r^2 from 0.16 to 0.76). Models performance within the calibration environment was generally similar regardless of the stage of measure-

Table 2
Main statistical parameters of the models

Model	N	PLSR factors	Calibration			Cross-validation		
			r^2	RMSE	rRMSE	r^2	RMSE	rRMSE
Anthesis								
6LR	100	7	0.79***	253	4.5	0.71***	300	5.4
6MR	100	3	0.76***	543	4.9	0.74***	568	5.1
6MI1	100	4	0.74***	940	5.2	0.67***	1049	5.8
6MI2	100	3	0.46***	562	7.3	0.41***	590	7.7
6HI	68	2	0.23***	613	8.4	0.16***	644	8.8
Milk-grain								
7LR	100	2	0.61***	349	6.2	0.58***	364	6.5
7MR	100	5	0.81***	484	4.4	0.76***	547	4.9
7MI1	100	1	0.71***	997	5.5	0.69***	1021	5.6
7MI2	98	4	0.61***	474	6.2	0.42***	578	7.5
7HI	99	2	0.20***	650	8.9	0.16***	671	9.2

N, number of samples; r^2, determination coefficient of the regression line between predicted and measured values; RMSE, root mean standard error (kg ha^{-1}); rRMSE, ratio between RMSE and the standard error of grain yield within each trial.
*** $P < 0.001$.

ment. Nevertheless, we found somewhat better fit in medium-yield trials with the models calibrated with spectra acquired at milk-grain stage, whereas for the drier environment (LR) the best predictions were found in anthesis.

3.3. General trends in models performance when comparing genotype yields

The usefulness of models to discriminate between the yield of different genotypes was evaluated using mean data of each genotype within each trial. Fig. 4 shows the relationship between predicted and harvested grain yield within the calibration trial (cross-validation values). The strongest and most consistent relationships were found within medium-yielding trials, specially at milk-grain stage (Fig. 4c and d). Within the low-yielding trial (LR) the relationship was only significant at anthesis, whereas the opposite was the case for the high-yielding trial (HI). In all cases, slope and intercept did not differ significantly from 1 and 0, respectively. Both RMSE and rRMSE for genotype means were generally smaller than for predicted plot values (data not shown). Nevertheless, the quantification of grain yield was still poor, with RMSE values being from three- to five-fold greater than the standard error across genotype means.

The robustness of the models was further tested by applying each one to all the trials assayed (see Fig. 5). The ability of PLSR models derived from VIS/NIR spectra for predicting grain yield of durum wheat varied with both developmental stage and trial where measures were taken. Fig. 5a shows that the five models constructed with anthesis spectra had similar predictive ability across the five trials. In contrast, we found greater differences in the response across trials among milk-grain models (Fig. 5b). PLSR models had generally better performance for predicting grain yield of durum wheat grown in trials with medium productivity potential. Indeed, most of the models, either from anthesis or milk-grain spectra, showed greater correlations between predicted and estimated mean genotype yield within the three trials of medium-yield potential (average correlation coefficient of both stages, $r = 0.65 \pm 0.09$) than within the low ($r = 0.41 \pm 0.13$) and high ($r = 0.42 \pm 0.17$) productivity trials (Fig. 5). On the other hand, the yield of the low productivity trial was best predicted by models constructed with anthesis spectra, whereas in the high productivity trial the best predictions were attained using milk-grain models.

The broad-sense heritability (H^2) of grain yield observed by harvesting was 0.33. The H^2 of estimated GY by PLSR was different across models, ranging from 0.1 to 0.25 and from 0.01 to 0.20 for milk-grain

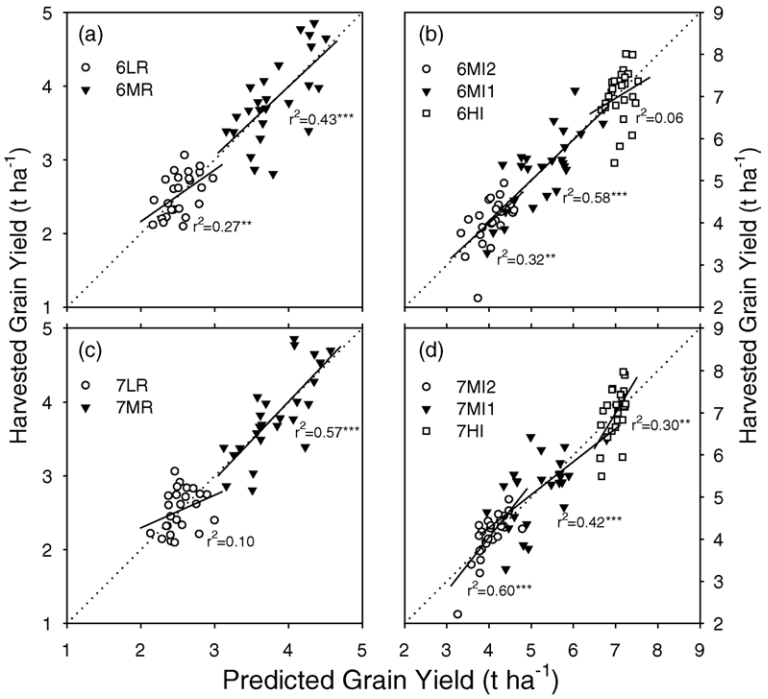

Fig. 4. Relationships between genotype means of measured (harvested) and predicted grain yield using data from the same trials where have been calibrated. Predicted values are those resulting from the cross-validation procedure: (a) and (b) anthesis models; (c) and (d) milk-grain models. 6LR, 7LR, models calibrated within the low-yielding, rainfed trial; 6MR, 7MR, models calibrated within the medium-yielding, rainfed trial; 6MI1, 6MI2, 7MI1, 7MI2, models calibrated within medium-yielding, irrigated trials; 6HI, 7HI, models calibrated within the high-yielding, irrigated trial.

and anthesis models, respectively (Fig. 6). In spite of the lack of a clear tendency, H^2 showed higher and more steady values in the models from milk-grain spectra (0.18 ± 0.06) than in those from anthesis (0.14 ± 0.08). In addition, within milk-grain model, the medium productivity environments had higher values (0.21 ± 0.05) than low and high productivity environments.

4. Discussion

4.1. Physiological background of the relationship between reflectance models and GY

Despite being an empirical approach, the models obtained by PLSR calibration were able to integrate physiological information from several spectral bands in order to estimate GY (Fig. 3). Indeed, among the highest regression coefficients, we found wavelengths previously included in spectral indices of green biomass and LAI (near-infrared/red, Peñuelas et al., 1997a), chlorophyll content (550–680 nm, Haboudane et al., 2002), water content (970 nm, Peñuelas et al., 1996) and carotenoids (430–445 nm, Peñuelas et al., 1995b). All models showed negative coefficients in the left side of the red edge region (λ_{RE}), where reflectance is reduced when the red/near-infrared slope increases and shifts towards the right (see Fig. 2). Filella and Peñuelas (1994) showed that this slope and its position were closely related to chlorophyll content, biomass and water status. The positive coefficients given by some models (6LR, 6HI, 7LR, 7HI) in the near-infrared region (750–950 nm), associated with the relative content of brown pigments (Peñuelas and Filella, 1998), might also be related with green biomass and water status. In addition, variability in water status was considered in all the

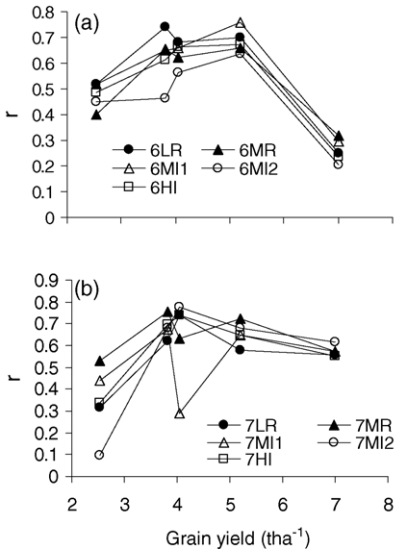

Fig. 5. Correlation coefficients between genotype means of measured and predicted grain yield for the models developed in each trial when applied to all the trials assayed, plotted against average yield of the application trial: (a) and (b) stand for models calibrated from anthesis and milk-grain spectra, respectively. 6LR, 7LR, models calibrated within the low-yielding, rainfed trial; 6MR, 7MR, models calibrated within the medium-yielding, rainfed trial; 6MI1, 6MI2, 7MI1, 7MI2, models calibrated within medium-yielding, irrigated trials; 6HI, 7HI, models calibrated within the high-yielding, irrigated trial.

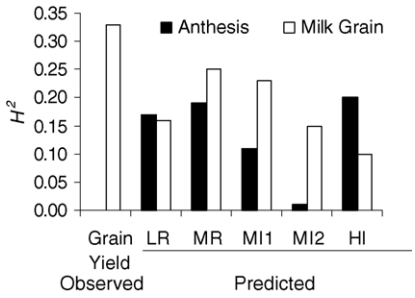

Fig. 6. Broad-sense heritabilities (calculated from data of all trials) for observed grain yield and predicted grain yield using PLSR models developed either from anthesis or milk-grain spectra. LR, models calibrated within the low-yielding, rainfed trial; MR, models calibrated within the medium-yielding, rainfed trial; MI1, MI2, models calibrated within medium-yielding, irrigated trials; HI, models calibrated within the high-yielding, irrigated trial.

models, by including negative coefficients around a secondary peak of water absorption (970 nm). The depletion of reflectance in this region has proven to be a good indicator of plant water content at the canopy level (Peñuelas et al., 1997b).

Other wavelengths accounted by the models were directly associated with chlorophyll absorption (450, 550–670 nm). Under low chlorophyll content in the canopy (e.g. due to drought or crop senescence) sensitivity is greater in absorption peaks (450, 670 nm). In contrast, for canopies with greater chlorophyll content, these absorption peaks become saturated, and the most sensitive spectral bands are placed around 550 nm (Peñuelas and Filella, 1998). Fig. 3 shows that at anthesis the regression coefficients at the maximum absorption peaks of chlorophyll shift from negative values at 6LR to values close to zero at 6MR and positive at 6HI, while the opposite trend was found for the 550 nm region. Given that the estimation of canopy chlorophyll content by crop reflectance depends on the product of green biomass and chlorophyll concentration at the leaf level (Filella et al., 1995), these results indicates that total photosynthetic capacity at anthesis increased from 6LR to 6MR and 6HI, likely saturating the spectra at the trial showing the highest biomass. On the other hand, from Fig. 3 it may be inferred that at trial MR senescence increased from anthesis to milk-grain stage (6MR and 7MR). At milk-grain stage negative values of the regression coefficients appeared around 670 nm, whereas they were positive in the blue domain (400–500 nm) at 7LR (see Fig. 3). In the blue region, both chlorophylls and carotenoids have high absorbances (Peñuelas and Filella, 1998). Provided negative coefficients in the region where only chlorophylls absorb (500–700 nm), the positive coefficients in the blue region might account for variations in the ratio between carotenoids and chlorophylls. This ratio is higher under stress and in senescing leaves, and decreases with higher nutrient availability (Filella et al., 1995). Thus, the pattern followed by the regression coefficients at milk-grain stage indicates that at 7LR the crop was far more senescent than at 7MR and 7HI.

In summary, according to the regression coefficients for the different spectral regions, our empirical models to estimate grain yield might account for three major constraints in GY: (1) photosynthetic size of the canopy (e.g. green biomass), through the near-infrared/red ratios, (2) water status, through the reflectance around 970 nm, and (3) nitrogen status,

as related with chlorophyll content and carotenoids to chlorophylls ratio.

4.2. Impact of biomass and crop senescence on the relationship between spectra and yield

The values of the r^2 of the calibration and validation models indicated that the amount of grain yield variability within a trial (across plots) explained by the models was greater in low and medium-yield environments with spectra captured either at anthesis or milk-grain stage (see Table 2). This result could be explained by the differences between trials in total and green biomass when spectra were captured, as confirmed by Fig. 3. Thus, the large biomass on HI trial probably saturated the spectra at red and infrared wavelengths, giving poor predictive assessment of yield both at anthesis or milk-grain. On the other hand, these results could be partially attributed also to the recorded large variability of yield between blocks in the poorest environments, which on increasing the range of data, improved the predictive value of the models at the plot level.

Moreover, a trial × growth stage interaction appeared for the determination coefficients of calibration models, given that r^2 was higher at low productivity than at moderate productivity environments at anthesis, the opposite being true at milk-grain stage. This result may be explained in terms of crop senescence, since at anthesis biomass at MR and MI were higher than at LR (see Section 4.1), probably saturating the spectra at some wavelengths, and thus the best appraisal of crop production was obtained at LR. Contrarily, at milk-grain stage, at MR and MI the crop had started to senesce, but still had a large photosynthetic capacity, able to contribute to grain yield. In contrast, at LR senescence was much advanced, limiting the ability of canopy reflectance to properly track changes in productivity.

4.3. Model usefulness for selection purposes

In general, when the relationships between predicted and observed grain yield were studied using mean values of genotypes for each trial, the best relationships were found in medium to high-yielding trials. On them, genotypes maximized their divergences in yield, giving more chance to the models to detect genotype differences (see Figs. 4 and 5). Nevertheless, even within the same trial used for calibration, RMSE values were far greater than the standard error of the data, and this error increased significantly when applying the models to other trials. The main consequence of such results is that spectral models of grain yield did not provide an accurate quantification of grain yield values. However, it should be taken into account that when screening within a large number of genotypes, breeders are more interested on the ranking of their yields, than in the accurate quantification of yield values. Provided the strongly significant relationship found between measured and modeled grain yield, reflectance models of grain yield could still be useful for breeding purposes. Indeed, the relationships between grain yield and our reflectance models were generally stronger than those found for previously suggested selection tools for yield improvement (Araus et al., 1998; Ferrio et al., 2004; Royo et al., 2002).

4.4. PLS models versus vegetation indices

Despite requiring empirical calibration, our models showed generally stronger and more robust relationships with grain yield than any of the previously assayed spectral indices (Aparicio et al., 2000; Royo et al., 2003). Indeed, both milk-grain and anthesis models attained high and steady performances in discriminating between genotype means (average $r = 0.66 \pm 0.1$ and $r = 0.64 \pm 0.1$, respectively). Aparicio et al. (2000) found similarly strong relationships between durum wheat yield and SR ($r = 0.63$), and NDVI ($r = 0.60$), but only when measured at anthesis for experiments under rainfed conditions, whereas for irrigated ones the best correlations were attained at maturity and were lower than those of rainfed environments ($r = 0.55$). In a similar way, Royo et al. (2003) found that the usefulness of reflectance indices for yield prediction were highly environmental-dependent. The most useful indices were R680, WI and SR, which had coefficients of correlation with yield of 0.11 to −0.68, 0.19 to −0.57, and 0.05–0.59, respectively, that are lower and unsteady than those found in this work. For our best model, correlation coefficients between genotype means of predicted and measured GY within each of the five trials ranged from 0.53 to 0.76.

4.5. Best environments and growth stage for measurements

The best performance of models for predicting the grain yield of durum wheat grown in environments with medium and high productivity was in concordance with that pointed out by Royo et al. (2003). They found that the ability of some spectral reflectance indices (i.e. water index) to predict yield of durum wheat was higher in locations where genotypes expressed their potential. In our results, the models built with spectra of milk-grain ranked adequately the yield of genotypes, not just from medium productivity, but also from high productivity environments. This could be useful for breeding programs, as selection for yield potential is usually carried out at locations from medium to high productivity that maximize the heritability of target traits.

Regarding the optimal crop stage for measurements, the models developed from either milk-grain or anthesis spectra showed similar responses as those reported for some spectral indices. The yield of the low productivity environment could be better ranked by measures taken at anthesis, which was also found by Aparicio et al. (2000) using the SR and NDVI indices. In contrast, within the medium to high-yielding trials, yield was better assessed by milk-grain models. This agrees with previous works showing better performance of vegetation indices when measured during grain filling in mid-high-yielding environments (Aparicio et al., 2000; Royo et al., 2003). Whereas under low-watered environments photosynthetic size of the canopy is already declining at anthesis, it can still remain or even increase under well-watered environments (Royo et al., 2004). Therefore, reflectance spectra measured after anthesis in the low-yielding environment did not provide additional information, but added extra noise from senescent leaves, whereas in the high-yielding environment, measures taken at anthesis failed to estimate the overall photosynthetic potential of the canopy, probably due to the saturation of spectra for leaf area index (LAI) values higher than 3 (Sellers, 1987). While Royo et al. (2003) using spectral indices (e.g. R680, WI, SR) established that milk-grain was the best stage for durum wheat yield appraisal, our results indicated that both anthesis and milk-grain spectra could be useful for yield assessment, depending on the productivity of the environment. However, the fact that the higher heritabilities were obtained at milk-grain, indicates that this is the best stage for yield assessment in locations from medium to high productivity, which are the most used for breeding programs in Mediterranean environments (Ceccarelli, 1989).

5. Concluding remarks

From these results, we can conclude that our empirical models, although not being accurate enough to quantify grain yield, could still provide a qualitative assessment of yield differences among genotypes. In general, the models obtained were robust enough to rank genotypes by their yield, even when applied to environments different from those used for calibration. Thus, our approach might be useful at the early generations of breeding programs, when yield trials are less feasible, in order to discard poor-yielding genotypes. The only limitation in this case would be the plot size needed for capturing the spectra. By integrating in the same model the miscellaneous information provided by several spectral regions, PLSR models developed from VIS/NIR spectra showed generally stronger and more robust assessments of grain yield than previously assayed spectral indices. Our results suggest that the most reliable ranking of genotypes can be attained within medium to high productivity environments. We also found that, in such environments, the most recommended stage for measurements was milk-grain. This technique could be especially useful for breeding purposes, as selection for yield is mostly performed on medium–high-yielding trials. Nevertheless, these models should be tested on a wider range of environments and genotypes in order to further assess their robustness.

Acknowledgments

This study was supported in part by the CICYT (Spain) research projects AGF96-1137-C02-01 and AGL-2002-04285. The skilled technical assistance of the staff of the Àrea de Conreus Extensius is gratefully acknowledged. We thank Dr. J. Puy, from the

Departament de Química of Universitat de Lleida, for his useful advises on multivariate calibration. We also thank J. Casadesús, from the Camps Experimentals of Universitat de Barcelona, for his technical tips on spectroradiometry. J.P. Ferrio is a recipient of a Ph.D. fellowship from the Generalitat de Catalunya.

Appendix A

Regression coefficients for each wavelength resulting from the models described in the paper. The coefficients should be applied to SNV reflectance spectra

Wavelength	Anthesis models					Milk-grain models				
	6LR	6MR	6MI1	6MI2	6HI	7LR	7MR	7MI1	7MI2	7HI
398.760	−300	40	128	−40	38	42	−130	81	173	39
400.195	−372	47	143	−43	37	41	−124	81	169	38
401.630	−458	40	149	−23	37	40	−124	80	198	38
403.064	−393	36	139	−65	38	40	−149	79	171	37
404.499	−465	39	124	−22	35	41	−133	79	185	38
405.934	−406	42	134	−67	35	39	−148	78	148	38
407.369	−385	39	128	−55	36	40	−152	77	94	38
408.804	−513	29	148	−16	33	38	−150	77	105	37
410.238	−467	31	139	−34	34	39	−162	76	142	36
411.673	−530	31	145	−39	36	39	−175	75	117	36
413.108	−465	33	137	−49	33	38	−149	74	88	35
414.543	−480	34	127	−44	33	38	−150	74	80	34
415.978	−493	29	128	−22	32	37	−182	73	62	34
417.412	−509	29	121	−50	31	37	−196	72	83	33
418.847	−534	32	117	−36	32	37	−189	71	43	32
420.282	−436	31	111	−45	31	37	−186	70	30	31
421.717	−432	26	102	−40	30	36	−199	69	21	31
423.152	−488	24	82	−36	30	35	−202	69	37	30
424.586	−480	23	70	−26	30	36	−211	68	23	29
426.021	−438	27	72	−29	28	34	−203	66	28	29
427.456	−418	28	60	−54	28	34	−213	66	28	28
428.891	−474	23	37	−29	28	33	−241	65	40	28
430.326	−493	21	57	−34	27	32	−216	64	46	27
431.760	−474	22	168	−31	27	33	−225	63	47	27
433.195	−469	18	160	−33	26	32	−221	63	31	26
434.630	−445	20	180	−45	25	32	−229	62	21	26
436.065	−501	17	179	−16	25	30	−249	62	38	25
437.500	−434	19	197	−26	26	30	−260	60	28	25
438.934	−448	16	208	−28	24	30	−247	60	11	25
440.369	−459	18	231	−35	24	30	−250	59	10	24
441.804	−391	19	216	−16	23	29	−272	58	−3	24
443.239	−464	18	242	−17	24	28	−260	57	0	23
444.674	−606	16	265	−14	23	28	−265	57	−9	22
446.108	−514	18	260	−16	23	27	−273	56	−27	22
447.543	−496	19	292	−24	23	27	−278	55	−13	22

Appendix A (*Continued*)

Wavelength	Anthesis models					Milk-grain models				
	6LR	6MR	6MI1	6MI2	6HI	7LR	7MR	7MI1	7MI2	7HI
448.978	−505	17	283	−10	23	26	−271	54	−30	21
450.413	−516	16	290	−18	22	25	−272	53	−22	21
451.848	−519	17	283	−13	22	26	−277	52	−20	21
453.282	−483	17	285	−12	22	25	−270	51	−23	21
454.717	−493	18	287	−20	22	24	−273	51	−31	20
456.152	−473	16	292	−9	22	24	−276	50	−20	20
457.587	−446	17	287	−15	21	24	−274	49	−23	19
459.022	−455	18	290	−6	20	24	−262	49	−39	19
460.456	−442	19	296	−18	21	23	−276	48	−18	19
461.891	−447	19	290	−12	21	23	−270	47	−22	19
463.326	−482	18	274	−11	21	22	−266	46	−31	19
464.761	−436	18	263	−11	21	22	−271	45	−32	19
466.196	−459	19	253	−5	20	22	−259	45	−37	19
467.630	−449	19	255	−18	20	22	−272	44	−43	19
469.065	−487	18	251	−5	20	21	−265	44	−20	19
470.500	−501	18	261	4	20	21	−260	43	−44	18
471.935	−492	19	254	−6	21	21	−264	42	−36	18
473.370	−501	19	255	−9	20	21	−263	41	−39	18
474.804	−494	20	250	−31	19	20	−261	41	−54	18
476.239	−529	19	253	−1	19	19	−267	40	−49	18
477.674	−554	19	255	−15	20	19	−275	39	−54	17
479.109	−527	20	244	−1	19	19	−257	39	−72	17
480.544	−556	19	239	−8	19	18	−261	38	−67	17
481.978	−580	22	235	−18	19	18	−262	38	−60	17
483.413	−580	20	185	−4	19	17	−270	37	−68	16
484.848	−575	21	190	−11	19	18	−269	36	−71	16
486.283	−603	22	204	−8	19	16	−257	35	−63	16
487.718	−588	22	233	−23	19	17	−245	35	−63	16
489.152	−618	23	220	−7	18	16	−241	34	−50	15
490.587	−620	23	224	2	18	15	−245	34	−43	15
492.022	−614	24	229	−6	18	15	−235	32	−57	15
493.457	−631	24	253	−8	18	14	−236	32	−53	15
494.892	−601	25	264	−15	17	13	−227	31	−53	14
496.326	−648	24	234	−7	17	12	−232	30	−39	14
497.761	−626	23	238	−1	17	13	−230	29	−63	13
499.196	−623	22	248	−7	17	12	−222	28	−58	13
500.631	−670	23	250	−3	15	11	−217	27	−65	13
502.066	−708	25	248	−7	15	10	−194	27	−50	12
503.500	−691	25	282	9	14	10	−200	25	−63	11
504.935	−683	23	294	4	14	10	−184	24	−69	10
506.370	−642	23	327	6	13	9	−179	23	−74	9
507.805	−695	23	330	6	12	8	−173	22	−68	8

Appendix A (*Continued*)

Wavelength	Anthesis models					Milk-grain models				
	6LR	6MR	6MI1	6MI2	6HI	7LR	7MR	7MI1	7MI2	7HI
509.240	−712	23	328	9	11	7	−159	21	−82	7
510.674	−643	21	349	21	10	6	−155	19	−87	5
512.109	−653	18	368	19	9	6	−147	17	−78	4
513.544	−654	18	368	16	8	6	−126	16	−81	3
514.979	−689	17	368	11	5	4	−118	15	−82	1
516.414	−496	15	387	29	5	3	−110	13	−70	−1
517.848	−705	12	447	37	3	3	−97	12	−81	−3
519.283	−586	9	497	27	1	3	−76	10	−78	−4
520.718	−567	7	530	41	−1	1	−68	9	−72	−6
522.153	−513	5	553	29	−3	0	−79	7	−69	−7
523.588	−471	0	585	38	−5	0	−67	6	−83	−9
525.022	−393	−2	619	49	−5	−1	−57	4	−76	−11
526.457	−355	−6	669	51	−8	−3	−53	3	−75	−12
527.892	−345	−7	716	55	−9	−3	−49	1	−76	−13
529.327	−327	−8	757	48	−11	−4	−52	0	−65	−14
530.762	−222	−13	791	58	−12	−4	−59	−1	−81	−16
532.196	−218	−14	818	58	−14	−6	−44	−3	−75	−17
533.631	−123	−15	846	66	−15	−6	−45	−5	−89	−19
535.066	−136	−17	880	68	−16	−7	−51	−6	−77	−20
536.501	−105	−17	916	62	−17	−8	−48	−8	−87	−21
537.936	−29	−20	936	77	−17	−9	−56	−9	−94	−22
539.370	−16	−22	947	66	−18	−10	−48	−10	−98	−23
540.805	24	−22	966	77	−19	−11	−33	−12	−87	−24
542.240	31	−24	1001	65	−20	−12	−32	−13	−84	−25
543.675	100	−25	1037	66	−20	−13	−42	−14	−79	−26
545.110	166	−26	1064	60	−21	−14	−35	−16	−80	−27
546.544	145	−26	1066	58	−22	−15	−38	−18	−98	−28
547.979	143	−28	1071	56	−22	−16	−19	−19	−95	−28
549.414	177	−28	1103	43	−23	−17	−31	−20	−85	−29
550.849	213	−27	1102	51	−23	−18	−19	−21	−74	−30
552.284	237	−28	1103	50	−25	−19	−27	−23	−81	−30
553.718	311	−30	1088	51	−24	−20	−12	−24	−69	−31
555.153	315	−27	1062	46	−25	−21	−26	−26	−64	−31
556.588	304	−26	1041	40	−24	−22	−23	−28	−65	−32
558.023	352	−25	1009	51	−24	−23	−31	−29	−63	−32
559.458	366	−24	983	44	−24	−23	−20	−30	−58	−31
560.892	325	−23	965	43	−24	−25	−7	−31	−49	−32
562.327	318	−20	930	39	−23	−26	−15	−33	−50	−32
563.762	275	−20	899	34	−24	−26	−16	−34	−47	−32
565.197	274	−17	851	47	−23	−27	−14	−35	−53	−32
566.632	256	−14	777	40	−23	−28	−11	−37	−61	−31
568.066	237	−13	731	39	−21	−28	−9	−38	−44	−31

Appendix A (*Continued*)

Wavelength	Anthesis models					Milk-grain models				
	6LR	6MR	6MI1	6MI2	6HI	7LR	7MR	7MI1	7MI2	7HI
569.501	195	−11	690	27	−21	−29	−10	−39	−40	−31
570.936	171	−7	635	32	−20	−29	−8	−40	−36	−31
572.371	253	−5	576	30	−19	−30	4	−41	−42	−30
573.806	166	−4	534	35	−18	−31	4	−42	−33	−30
575.240	151	−1	475	35	−18	−31	−6	−43	−21	−29
576.675	105	3	435	33	−17	−32	−1	−44	−18	−29
578.110	136	5	383	33	−16	−33	−1	−45	−22	−29
579.545	160	6	339	34	−16	−33	0	−46	−25	−28
580.980	143	6	315	35	−16	−34	7	−47	−7	−28
582.414	120	9	282	29	−15	−34	−4	−47	−5	−28
583.849	164	11	250	27	−15	−35	−2	−48	−7	−28
585.284	88	12	179	44	−15	−35	2	−49	−6	−28
586.719	84	13	131	54	−15	−36	−1	−50	−7	−27
588.154	−10	13	84	55	−15	−37	−1	−51	6	−27
589.588	−71	15	38	47	−14	−37	−5	−52	3	−27
591.023	−57	16	45	45	−14	−37	6	−53	2	−28
592.458	−94	16	13	53	−14	−37	0	−54	1	−27
593.893	−121	15	−15	42	−13	−38	2	−55	9	−27
595.328	−190	17	−30	47	−14	−38	4	−56	5	−27
596.762	−172	18	−48	41	−14	−39	−1	−56	4	−28
598.197	−182	17	−80	47	−12	−38	−2	−57	−11	−28
599.632	−230	16	−100	55	−14	−39	0	−58	−4	−27
601.067	−249	18	−121	46	−14	−40	0	−59	1	−28
602.502	−184	19	−125	43	−13	−40	5	−59	−11	−28
603.936	−263	19	−125	46	−13	−39	7	−60	−14	−28
605.371	−179	20	−158	52	−13	−40	2	−61	−10	−28
606.806	−199	21	−179	45	−13	−41	8	−61	6	−27
608.241	−210	22	−185	57	−12	−40	15	−61	5	−27
609.676	−194	25	−186	49	−12	−40	20	−62	8	−26
611.110	−186	25	−210	51	−10	−40	24	−62	2	−26
612.545	−187	25	−227	57	−10	−41	24	−62	11	−25
613.980	−210	26	−231	52	−10	−41	43	−63	36	−25
615.415	−209	29	−249	51	−10	−41	33	−63	26	−25
616.850	−249	30	−242	46	−9	−41	27	−64	32	−24
618.284	−301	31	−265	47	−8	−41	35	−64	37	−24
619.719	−311	31	−292	52	−9	−41	34	−64	48	−24
621.154	−222	29	−351	44	−8	−41	30	−65	48	−24
622.589	−227	33	−326	55	−8	−41	26	−66	33	−24
624.024	−353	33	−329	54	−8	−42	16	−66	25	−24
625.458	−99	33	−366	52	−9	−42	18	−67	−1	−24
626.893	−298	30	−387	55	−7	−42	23	−68	23	−23
628.328	−328	33	−359	62	−8	−42	21	−69	13	−24
629.763	−355	34	−357	52	−7	−43	3	−69	8	−24

Appendix A (*Continued*)

Wavelength	Anthesis models					Milk-grain models				
	6LR	6MR	6MI1	6MI2	6HI	7LR	7MR	7MI1	7MI2	7HI
631.198	−352	33	−381	43	−7	−43	15	−70	5	−25
632.632	−387	31	−413	43	−8	−43	19	−70	−8	−24
634.067	−389	33	−374	45	−7	−43	22	−71	3	−24
635.502	−447	33	−421	45	−7	−43	2	−71	−31	−24
636.937	−471	35	−437	36	−7	−44	2	−71	−25	−24
638.372	−528	35	−441	24	−7	−44	−15	−72	−15	−24
639.806	−599	37	−472	23	−7	−44	−7	−72	3	−23
641.241	−672	38	−492	25	−6	−43	−17	−72	−14	−22
642.676	−717	43	−515	26	−6	−44	−25	−72	−26	−22
644.111	−767	42	−522	10	−5	−45	−34	−73	−33	−21
645.546	−804	46	−567	24	−4	−45	−33	−72	−27	−21
646.980	−873	43	−568	22	−4	−45	−55	−73	−6	−20
648.415	−873	47	−593	13	−3	−44	−50	−73	−18	−19
649.850	−887	48	−600	25	−4	−45	−46	−73	−15	−19
651.285	−812	49	−619	−2	−3	−45	−42	−73	−20	−18
652.720	−768	48	−605	26	−3	−45	−44	−74	−8	−18
654.154	−687	49	−595	28	−3	−45	−50	−74	−12	−18
655.589	−674	47	−601	30	−3	−45	−75	−75	−22	−17
657.024	−610	53	−584	30	−1	−46	−69	−74	−33	−17
658.459	−554	51	−574	10	−1	−45	−58	−73	−11	−16
659.894	−517	53	−576	8	0	−45	−51	−73	−12	−16
661.328	−468	56	−582	18	0	−45	−56	−72	−30	−16
662.763	−439	55	−587	21	0	−45	−66	−72	−15	−15
664.198	−366	57	−600	17	2	−45	−84	−72	−21	−15
665.633	−359	57	−597	7	1	−44	−80	−71	−3	−14
667.068	−331	59	−585	22	2	−44	−78	−71	−20	−14
668.502	−333	58	−587	18	3	−45	−86	−71	−16	−13
669.937	−314	60	−581	20	3	−45	−104	−71	−17	−13
671.372	−207	63	−602	9	4	−45	−113	−71	−10	−12
672.807	−220	60	−582	4	3	−46	−100	−71	23	−12
674.242	−177	60	−587	25	2	−44	−102	−71	−10	−12
675.676	−168	58	−598	24	3	−45	−108	−72	−15	−12
677.111	−102	62	−592	23	2	−46	−104	−72	8	−12
678.546	−65	60	−584	16	4	−45	−114	−73	24	−12
679.981	−79	57	−594	24	3	−45	−109	−74	15	−13
681.416	−51	60	−576	35	2	−46	−96	−76	−6	−14
682.850	−50	58	−583	37	1	−46	−86	−78	30	−14
684.285	111	56	−569	33	1	−47	−85	−80	23	−16
685.720	109	54	−547	24	−1	−48	−48	−84	35	−18
687.155	180	50	−538	61	−3	−48	−26	−88	52	−20
688.590	159	45	−524	56	−6	−48	−1	−91	46	−23
690.024	128	41	−514	41	−7	−50	32	−96	58	−28
691.459	245	32	−483	67	−11	−52	53	−100	37	−32

Appendix A (*Continued*)

Wavelength	Anthesis models					Milk-grain models				
	6LR	6MR	6MI1	6MI2	6HI	7LR	7MR	7MI1	7MI2	7HI
692.894	187	23	−461	73	−16	−52	75	−105	58	−37
694.329	190	11	−408	80	−21	−54	88	−110	11	−42
695.764	160	−2	−365	83	−26	−55	112	−115	29	−48
697.198	162	−13	−298	89	−28	−57	111	−120	11	−53
698.633	248	−29	−237	102	−35	−58	129	−125	12	−59
700.068	234	−46	−199	99	−41	−59	136	−129	−10	−65
701.503	134	−64	−162	125	−48	−61	126	−134	−31	−70
702.938	137	−82	−108	113	−52	−63	127	−138	−31	−76
704.372	205	−92	−73	116	−57	−64	106	−141	−61	−80
705.807	12	−112	−53	102	−64	−64	88	−145	−57	−85
707.242	−46	−132	−43	107	−69	−65	51	−148	−107	−89
708.677	−101	−147	−21	100	−74	−66	31	−150	−91	−94
710.112	−245	−163	−30	91	−77	−66	−19	−152	−137	−98
711.546	−175	−178	−22	88	−84	−67	−54	−154	−148	−102
712.981	−297	−198	−48	87	−90	−67	−65	−156	−181	−106
714.416	−368	−215	−43	70	−94	−67	−105	−157	−224	−110
715.851	−478	−226	−25	74	−99	−67	−149	−158	−220	−114
717.286	−490	−245	−1050	73	−104	−68	−199	−157	−282	−118
718.720	−627	−262	−888	65	−110	−67	−258	−156	−324	−122
720.155	−618	−282	−1179	55	−116	−66	−251	−154	−348	−125
721.590	−635	−292	−1118	8	−119	−66	−287	−151	−379	−127
723.025	−808	−307	−1308	5	−122	−66	−312	−148	−393	−129
724.460	−700	−314	−1476	−6	−127	−65	−367	−143	−376	−130
725.894	−822	−328	−1445	−47	−131	−63	−383	−137	−437	−130
727.329	−871	−335	−1521	−71	−132	−62	−399	−130	−420	−129
728.764	−833	−336	−1700	−58	−134	−60	−424	−122	−401	−128
730.199	−846	−341	−1956	−87	−132	−60	−430	−113	−412	−125
731.634	−789	−336	−1531	−117	−132	−58	−450	−102	−394	−120
733.068	−843	−334	−878	−159	−130	−55	−435	−91	−426	−116
734.503	−782	−325	−495	−163	−125	−53	−425	−80	−393	−110
735.938	−775	−314	−564	−151	−123	−51	−413	−68	−333	−103
737.373	−759	−302	−814	−173	−117	−50	−414	−54	−332	−95
738.808	−764	−285	−954	−167	−111	−48	−403	−41	−312	−88
740.242	−645	−267	−1031	−194	−102	−45	−355	−28	−285	−79
741.677	−655	−251	−923	−186	−95	−43	−379	−14	−232	−70
743.112	−642	−231	−755	−182	−87	−42	−339	−2	−252	−61
744.547	−620	−209	−698	−165	−76	−41	−319	11	−206	−53
745.982	−692	−187	−739	−165	−69	−38	−301	23	−184	−44
747.416	−571	−169	−937	−165	−58	−36	−272	35	−193	−36
748.851	−544	−147	−1250	−147	−49	−35	−257	45	−149	−29
750.286	−568	−131	−1593	−146	−41	−34	−252	55	−165	−21
751.721	−485	−107	−1651	−120	−33	−32	−228	64	−131	−15
753.156	−452	−96	−1697	−95	−24	−30	−193	72	−111	−8

Appendix A (*Continued*)

Wavelength	Anthesis models					Milk-grain models				
	6LR	6MR	6MI1	6MI2	6HI	7LR	7MR	7MI1	7MI2	7HI
754.590	−490	−80	−1668	−111	−17	−28	−188	78	−117	−3
756.025	−540	−65	−814	−88	−12	−28	−152	85	−84	2
757.460	−408	−60	−155	−109	−8	−26	−54	90	−114	7
758.895	−51	−37	−5	−100	−4	−24	−80	95	−115	11
760.330	−369	−7	−40	33	3	−25	−121	104	−125	16
761.764	−13	8	288	6	5	−22	−40	108	−145	21
763.199	95	11	258	6	11	−23	−35	109	−142	21
764.634	−65	12	47	8	12	−21	−51	110	−120	22
766.069	−222	9	31	11	17	−20	−66	110	−106	23
767.504	−199	5	−48	−9	19	−21	−43	111	−43	24
768.938	−251	9	−64	16	21	−19	−47	111	−12	25
770.373	−304	9	−105	29	23	−19	−54	111	−5	26
771.808	−172	15	−109	31	24	−18	−47	112	−4	27
773.243	−221	13	−106	18	26	−17	−18	113	−53	27
774.678	−165	14	−119	23	26	−15	−31	112	15	28
776.112	−153	18	−111	31	29	−15	−37	113	3	28
777.547	−127	16	−99	42	30	−14	−37	113	4	28
778.982	−98	23	−99	21	29	−14	−44	113	3	29
780.417	−222	24	−79	52	31	−12	−18	112	2	28
781.852	−48	19	−82	45	31	−12	−35	111	−9	28
783.286	−81	25	−74	36	32	−11	−9	111	−21	27
784.721	62	20	−40	27	32	−10	−5	112	−54	27
786.156	−8	26	−24	63	31	−7	1	111	−24	26
787.591	−27	25	−28	73	31	−8	25	110	−58	26
789.026	138	23	0	67	31	−7	6	110	−22	26
790.460	30	26	0	102	32	−7	13	109	−41	25
791.895	106	25	−53	74	32	−6	22	109	−14	26
793.330	178	27	−10	96	34	−5	29	108	−22	26
794.765	53	23	−17	86	32	−3	35	107	9	26
796.200	257	27	−18	77	35	−4	57	107	−4	26
797.634	214	26	−6	100	33	−2	76	106	32	25
799.069	219	27	−7	105	32	0	64	105	16	26
800.504	227	26	25	116	33	1	71	105	11	25
801.939	244	26	25	102	34	0	64	104	41	26
803.374	232	28	−14	121	35	0	89	104	22	25
804.808	461	23	−55	98	34	2	79	103	7	25
806.243	351	29	−38	104	32	2	81	102	34	25
807.678	405	24	−10	112	33	4	84	102	33	24
809.113	384	23	−1	107	34	4	91	101	15	24
810.548	337	27	60	144	35	4	100	100	15	23
811.982	423	25	131	119	31	5	106	99	10	22
813.417	431	27	249	168	32	8	142	99	−21	20
814.852	464	17	342	174	33	7	163	99	−69	18

Appendix A (*Continued*)

Wavelength	Anthesis models					Milk-grain models				
	6LR	6MR	6MI1	6MI2	6HI	7LR	7MR	7MI1	7MI2	7HI
816.287	394	18	312	190	33	8	133	98	−73	16
817.722	513	26	284	213	30	9	142	97	−118	17
819.156	532	30	217	165	29	10	105	95	−40	18
820.591	437	31	170	220	32	11	119	94	−44	18
822.026	486	15	232	151	33	11	175	94	−84	19
823.461	404	25	136	187	31	13	102	92	−119	16
824.896	490	19	82	204	29	13	94	92	−59	16
826.330	534	22	139	154	29	15	135	90	−12	17
827.765	397	16	152	183	29	13	169	89	−37	16
829.200	374	14	117	159	32	14	122	88	−27	16
830.635	475	15	91	161	28	15	142	85	−59	15
832.070	370	7	69	154	26	15	102	85	−46	16
833.504	403	13	35	181	30	17	104	84	19	15
834.939	407	6	10	167	28	18	109	83	12	16
836.374	253	7	−44	140	28	18	82	82	59	15
837.809	366	5	−76	155	27	19	65	80	12	15
839.244	375	3	−64	125	26	19	32	80	−7	16
840.678	410	0	−77	149	29	20	27	79	−37	14
842.113	296	0	−88	117	28	20	45	77	−36	15
843.548	228	−2	−100	134	26	21	70	77	−25	15
844.983	227	−3	−125	139	25	23	20	76	−22	13
846.418	281	8	−152	154	29	24	−25	75	−76	14
847.852	148	−7	−145	152	28	23	72	74	−30	13
849.287	5	−10	−111	112	28	24	25	74	−60	14
850.722	298	−5	−139	166	26	26	29	72	−72	13
852.157	436	−10	−167	150	30	26	16	72	−73	13
853.592	160	−4	−34	106	28	27	50	72	−61	14
855.026	338	−3	−170	187	27	27	83	69	−101	12
856.461	350	−5	−297	156	30	27	6	69	−50	12
857.896	38	−10	−150	139	26	28	24	67	2	13
859.331	192	−9	−117	117	30	28	37	68	−50	14
860.766	67	−9	−147	130	28	31	46	67	22	14
862.200	197	−9	−180	135	28	31	86	66	54	13
863.635	84	−15	−192	129	27	33	12	65	58	13
865.070	20	−16	−111	129	25	32	89	66	74	15
866.505	29	−5	−66	101	29	35	68	64	−2	13
867.940	38	−2	−208	153	24	32	1	63	4	12
869.374	60	−12	−210	163	28	33	25	61	−39	12
870.809	156	−15	−125	147	27	35	36	60	−14	11
872.244	12	−24	−142	121	27	33	22	60	−3	14
873.679	29	−7	−168	94	28	34	8	59	−25	9
875.114	−96	−12	−205	134	24	35	20	59	−13	10
876.548	100	−24	−129	149	25	39	−45	58	−66	10

Appendix A (*Continued*)

Wavelength	Anthesis models					Milk-grain models				
	6LR	6MR	6MI1	6MI2	6HI	7LR	7MR	7MI1	7MI2	7HI
877.983	−136	−6	−133	191	27	39	−4	56	−24	9
879.418	62	−19	−122	111	27	37	−52	57	−130	9
880.853	−2	−22	−148	141	25	37	−17	54	−139	8
882.288	134	−13	−170	158	27	39	−47	54	−57	8
883.722	−108	−25	−184	98	23	40	−27	53	−70	8
885.157	−71	−21	−165	122	20	40	8	52	−167	8
886.592	124	−18	−119	85	26	40	−25	51	−50	6
888.027	−316	−7	−190	163	24	40	−37	50	5	7
889.462	−407	−32	−224	118	25	38	5	49	−4	7
890.896	−224	−28	−84	58	20	39	−20	46	20	8
892.331	−120	−30	−84	109	23	41	31	47	−95	8
893.766	−358	−20	−22	66	17	42	28	46	−38	6
895.201	−222	−28	52	199	24	41	81	45	35	5
896.636	−293	−35	158	99	19	41	54	44	81	4
898.070	−52	−29	260	104	21	46	46	42	−86	2
899.505	−149	−25	373	167	16	40	54	43	−23	3
900.940	211	−17	333	182	13	42	111	41	−51	1
902.375	96	−20	207	247	22	45	−23	40	3	−1
903.810	−195	−26	151	153	14	44	−102	37	−55	−1
905.244	−185	−12	−32	175	13	44	−141	37	−217	0
906.679	−140	−32	144	179	17	45	38	36	−192	0
908.114	−644	−30	291	149	20	41	−102	36	−259	−1
909.549	−466	−32	252	141	16	46	106	36	−209	−3
910.984	−426	−19	263	146	17	43	−41	31	−392	−4
912.418	−139	−26	255	231	8	43	−104	31	−249	−1
913.853	−269	−22	339	125	16	40	33	31	−288	−6
915.288	−364	−34	272	203	24	39	105	29	−247	−3
916.723	−320	−47	281	120	8	41	84	29	−138	−4
918.158	−130	−24	225	108	2	34	34	25	−227	−4
919.592	−306	−24	178	182	14	42	31	25	−214	−6
921.027	−101	−15	−1	114	8	48	−10	23	16	−6
922.462	−529	−42	−30	176	15	46	−31	22	−32	−3
923.897	−357	−78	−5	12	6	44	−102	20	65	−3
925.332	−177	−25	101	63	8	38	−159	19	−76	−1
926.766	−99	−51	−26	136	14	45	−113	19	−58	−5
928.201	−557	−34	86	173	4	42	14	14	109	−5
929.636	−343	−63	337	151	8	43	−22	14	125	−6
931.071	−767	−59	528	−18	−2	34	23	10	−94	−7
932.506	−405	−34	966	100	13	43	262	10	132	0
933.940	−208	18	1115	−112	10	45	636	9	66	−9
935.375	−278	30	1157	206	25	25	765	2	−227	−5
936.810	−446	31	1175	241	−7	22	964	−10	−384	3

Appendix A (*Continued*)

Wavelength	Anthesis models					Milk-grain models				
	6LR	6MR	6MI1	6MI2	6HI	7LR	7MR	7MI1	7MI2	7HI
938.245	1530	95	1277	210	32	33	593	−14	−68	10
939.680	1027	36	850	470	6	25	293	−17	−307	−10
941.114	247	10	571	348	−3	30	486	−15	183	−13
942.549	−752	5	417	462	−3	28	227	−23	−359	−17
943.984	−195	−49	771	−88	−30	41	34	−24	−832	−21
945.419	1309	−23	789	195	−4	32	278	−28	−4	−11
946.854	1270	−25	556	220	0	33	794	−23	−404	−12
948.288	−516	31	500	268	1	32	667	−34	−11	−1
949.723	526	58	500	309	−20	5	372	−36	−153	2
951.158	969	−13	734	−132	−26	28	56	−44	−211	−3
952.593	697	−12	390	338	−23	20	538	−50	180	−10
954.028	−321	−41	325	3	−41	12	558	−49	−66	−19
955.462	−133	9	183	132	−51	10	490	−55	−497	−15
956.897	399	−106	209	106	−46	5	280	−66	−141	−7
958.332	1023	−75	67	−272	−28	7	118	−76	118	−22
959.767	375	−78	−40	128	−36	9	38	−74	127	−23
961.202	−696	−56	−455	−106	−57	10	274	−78	−16	−29
962.636	−490	−99	−126	238	−67	1	−223	−80	−267	−33
964.071	339	−114	−122	−200	−31	2	−416	−87	88	−38
965.506	727	−120	−384	−116	−77	3	−439	−95	−349	−37
966.941	−640	−135	−703	−435	−61	−8	−411	−86	−417	−50
968.376	523	−122	−757	−257	−65	−12	−447	−93	−508	−46
969.810	453	−89	−648	143	−65	−11	−650	−100	−465	−40
971.245	417	−101	−905	−411	−61	−13	−758	−101	−327	−46
972.680	−163	−166	−785	−150	−50	−6	−1018	−94	−1007	−45
974.115	−932	−158	−918	−380	−77	−3	−643	−93	−909	−48
975.550	−1098	−137	−980	−155	−57	−16	−785	−94	−759	−51
976.984	−578	−215	−914	−146	−63	−9	−641	−104	−210	−53
978.419	−125	−192	−704	−577	−60	−2	−558	−106	−632	−50
979.854	−965	−136	−1054	−221	−62	−30	−608	−98	−1283	−44
981.289	−508	−133	−1023	−316	−47	0	−636	−101	−347	−38
982.724	−708	−108	−883	19	−45	−22	−368	−109	−191	−38
984.158	461	−157	−937	−130	−76	−29	−542	−104	−23	−38
985.593	−798	−174	−992	−298	−56	−11	−874	−108	−193	−31
987.028	−582	−164	−1103	−350	−70	−27	−456	−104	165	−42
988.463	699	−115	−1207	−423	−52	0	−823	−104	−17	−35
989.898	−1001	−127	−1182	31	−52	−9	−710	−105	−141	−43
991.332	445	−171	−1309	−411	−70	−5	−712	−113	184	−44
992.767	−1297	−109	−1018	−383	−55	−14	−1219	−105	−740	−41
994.202	−1215	−172	−1267	−562	−51	2	−563	−101	225	−42
995.637	−367	−83	−1035	−344	−34	−36	−640	−103	−28	−40
997.072	−326	−147	−924	97	−80	−18	−722	−103	−504	−35

Appendix A (*Continued*)

Wavelength	Anthesis models					Milk-grain models				
	6LR	6MR	6MI1	6MI2	6HI	7LR	7MR	7MI1	7MI2	7HI
998.506	−72	−154	−1065	−683	−45	6	−801	−114	−705	−31
999.941	−1485	−107	−1280	−237	−54	−23	−882	−106	−752	−45
1001.380	872	−55	−1199	−459	−35	4	−575	−108	115	−50

References

Aparicio, N., Villegas, D., Araus, J.L., Casadesús, J., Royo, C., 2002. Relationship between growth traits and spectral vegetation indices in durum wheat. Crop Sci. 42, 1547–1555.

Aparicio, N., Villegas, D., Casadesús, J., Araus, J.L., Royo, C., 2000. Spectral vegetation indices as nondestructive tools for determining durum wheat yield. Agron. J. 92, 83–91.

Aparicio, N., Villegas, D., Royo, C., Casadesús, J., Araus, J.L., 2004. Effect of sensor view angle on the assessment of agronomic traits by ground level hyper-spectral reflectance measurements in durum wheat under contrasting Mediterranean conditions. Int. J. Remote Sens. 25, 1131–1152.

Araus, J.L., Amaro, T., Casadesús, J., Asbati, A., Nachit, M.M., 1998. Relationships between ash content, carbon isotope discrimination and yield in durum wheat. Aust. J. Plant Physiol. 25, 835–842.

Barnes, R.J., Dhanoa, M.S., Lister, S.J., 1989. Standard normal variate transformation and de-trending of near-infrared diffuse reflectance spectra. Appl. Spectrosc. 43, 772–777.

Bauer, M.E., 1975. The role of remote sensing in determining the distribution and yield of crops. Adv. Agron. 27, 271–304.

Beebe, K.R., Kowalski, B.R., 1987. An introduction to multivariate calibration and analysis. Anal. Chem. 59, 1007A–1017A.

Bort, J., Casadesús, J., Araus, J.L., Grando, S., Ceccarelli, S., 2002. Spectral vegetation indices as nondestructive indicators of barley yield in Mediterranean rain-fed conditions. In: Slafer, G.A., Molina-Cano, J.L., Savin, R., Araus, J.L., Romagosa, I. (Eds.), Barley Science: Recent Advances from Molecular Biology to Agronomy of Yield and Quality. Haworth Press, Binghamton, NH, pp. 387–412.

Ceccarelli, S., 1989. Wide adaptation: how wide? Euphytica 40, 197–205.

Ferrio, J.P., Bertran, E., Nachit, M.M., Català, J., Araus, J.L., 2004. Estimation of grain yield by near-infrared reflectance spectroscopy in durum wheat. Euphytica 137, 373–380.

Field, C.B., Gamon, J.A., Peñuelas, J., 1994. Remote sensing of terrestrial photosynthesis. In: Schulze, D.C., Caldwell, M.M. (Eds.), Ecophysiology of Photosynthesis. Springer-Verlag, Berlin, pp. 511–528.

Filella, I., Peñuelas, J., 1994. The red edge position and shape as indicators of plant chlorophyll content, biomass and hydric status. Int. J. Remote Sens. 15, 1459–1470.

Filella, I., Serrano, L., Serra, J., Peñuelas, J., 1995. Evaluating wheat nitrogen status with canopy reflectance indices and discriminant analysis. Crop Sci. 35, 1400–1405.

Gamon, J.A., Field, C.B., Goulden, M.L., Griffin, K.L., 1995. Relationships between NDVI, canopy structure, and photosynthesis in three Californian vegetation types. Ecol. Appl. 5, 28–41.

Gamon, J.A., Serrano, L., Surfus, J.S., 1997. The photochemical reflectance index: an optical indicator of photosynthetic radiation use efficiency across species, functional types, and nutrient levels. Oecologia 112, 492–501.

Haboudane, D., Miller, J.R., Tremblay, N., Zarco-Tejada, P.J., Dextraze, L., 2002. Integrated narrow-band vegetation indices for prediction of crop chlorophyll content for application to precision agriculture. Remote Sens. Environ. 81, 416–426.

Martens, H., Naes, T., 1991. Multivariate Calibration. Wiley, New York.

Peñuelas, J., Baret, F., Filella, I., 1995a. Semi-empirical indices to assess carotenoids/chlorophyll a ratio from leaf spectral reflectance. Photosynthetica 31, 221–230.

Peñuelas, J., Filella, I., Lloret, P., Muñoz, F., Vilajeliu, M., 1995b. Reflectance assessment of plant mite attack on apple trees. Int. J. Remote Sens. 14, 1887–1905.

Peñuelas, J., Filella, I., 1998. Visible and near-infrared reflectance techniques for diagnosing plant physiological status. Trends Plant Sci. 3, 151–156.

Peñuelas, J., Filella, I., Serrano, L., 1996. Cell wall elasticity and water index (R970 nm/R990 nm) in wheat under different nitrogen availabilities. Int. J. Remote Sens. 17, 373–382.

Peñuelas, J., Isla, R., Filella, I., Araus, J.L., 1997a. Visible and near-infrared reflectance assessment of salinity effects on barley. Crop Sci. 37, 198–202.

Peñuelas, J., Piñol, J., Ogaya, R., Filella, I., 1997b. Estimation of plant water concentration by the reflectance water index WI (R900/R970). Int. J. Remote Sens. 18, 2869–2875.

Raun, W.R., Solie, J.B., Johnson, G.V., Stone, M.L., Lukina, E.V., Thomason, W.E., Schepers, J.S., 2001. In-season prediction of potential grain yield in winter wheat using canopy reflectance. Agron. J. 93, 131–138.

Richardson, A.D., Berlyn, G.P., Gregoire, T.G., 2001. Spectral reflectance of *Picea rubens* (Pinaceae) and *Abies balsamea* (Pinaceae) needles along an elevational gradient, Mt. Moosilauke, New Hampshire, USA. Am. J. Bot. 88, 667–676.

Royo, C., Aparicio, N., Blanco, R., Villegas, D., 2004. Leaf and green area development of durum wheat genotypes grown under Mediterranean conditions. Eur. J. Agron. 20, 419–430.

Royo, C., Aparicio, N., Villegas, D., Casadesús, J., Monneveux, P., Araus, J.L., 2003. Usefulness of spectral reflectance indices as durum wheat yield predictors under contrasting Mediterranean environments. Int. J. Remote Sens. 24, 4403–4419.

Royo, C., Villegas, D., García del Moral, L.F., El Hani, S., Aparicio, N., Rharrabti, Y., Araus, J.L., 2002. Comparative performance of carbon isotope discrimination and canopy temperature depression as predictors of genotype differences in durum wheat yield in Spain. Aust. J. Agric. Res. 53, 561–569.

SAS Institute Inc., 1987. SAS/STAT™ Guide for Personal Computer, 6th ed. SAS, Cary, NC.

Sellers, P.J., 1987. Canopy reflectance, photosynthesis, and transpiration. II. The role of biophysics in the linearity of their interdependence. Remote Sens. Environ. 21, 143–183.

Serrano, L., Filella, I., Peñuelas, J., 2000. Remote sensing of biomass and yield of winter wheat under different nitrogen supplies. Crop Sci. 40, 723–731.

Vaesen, K., Gilliams, S., Nackaerts, K., Coppin, P., 2001. Ground-measured spectral signatures as indicators of ground cover and leaf area index: the case of paddy rice. Field Crops Res. 69, 13–25.

Walburg, G., Bauer, M.E., Daughtry, C.S.T., Housley, T.L., 1982. Effects of nitrogen on the growth, yield and reflectance characteristics of corn. Agron. J. 74, 677–683.

Wold, S., 1978. Cross validatory estimation of the number of components in factor and principal components models. Technometrics 20, 397–406.

Zadoks, J.C., Chang, T.T., Konzak, C.F., 1974. A decimal code for the growth stage of cereals. Weed Res. 14, 415–421.